CRYSTAL GROWTH & DESIGN

pubs.acs.org/crystal

Communication

Synthesis of Ultrathin Perovskite Nanowires via a Postsynthetic Transformation Reaction of Zero-Dimensional Perovskite Nanocrystals

Published as part of a Crystal Growth and Design virtual special issue on Nonclassical Crystallization in Synthetic and Natural Systems

Hanjun Yang, Tong Cai, Lacie Dube, Katie Hills-Kimball, and Ou Chen*

Cite This: *Cryst. Growth Des.* 2021, 21, 1924−1930

Read Online

ACCESS | Metrics & More | Article Recommendations | Supporting Information

ABSTRACT: The synthesis of lead-halide perovskite (LHP) thin nanowires (NWs) has been a challenging task that requires delicate control of nanocrystal (NC) nucleation and growth processes. Herein, we present a novel synthesis of ultrathin $CsPbBr_3$ NWs through a postsynthetic transformation reaction starting from zero-dimensional Cs_4PbBr_6 perovskite NCs. The synthesized $CsPbBr_3$ NWs averaged 2.5 nm in width and tens of micrometers in length, showing a blue photoluminescence with an emission quantum yield of 15.2%. Mechanistic studies show that the morphology of the final transformation product is determined by the chain length of the capping ligand and thus the formed template structure of the $PbBr_2$-ligand intermediates. We demonstrate that this reaction scheme can be applied to the synthesis of $CsPbI_3$ NCs with a low-dimensional morphology. Our study provides not only a new route to achieve ultrathin LHP NWs postsynthesis but also insights into the template-related nucleation and growth mechanisms of LHP NCs.

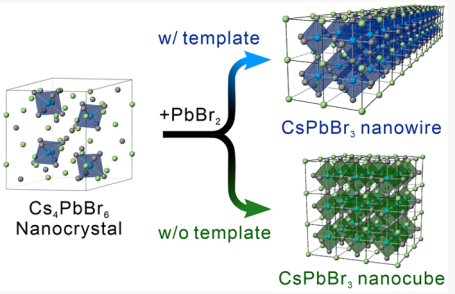

In the past decade, lead-halide perovskites (LHPs) have been rapidly developed as one of the most promising semiconductor materials for a wide range of applications, including solar cells,[1−5] light-emitting diodes,[6−8] photodetectors,[9−11] X-ray imaging,[12,13] etc.[14−18] In addition to the advantageous characteristics of bulk materials,[19] LHP nanocrystals (NCs) exhibit additional intriguing optical and electronic behaviors such as tunable optical spectral profiles,[20−23] high photoluminescence quantum yields (PL QYs),[24] superior single-particle emitting property,[25] unique assembly induced superfluorescence,[26] etc.[27] Because of their relatively small Bohr radius and thus weak quantum confinement of typical isotropic LHP NCs,[28] synthesizing LHP NCs with highly anisotropic morphologies represents an important means to regulate their desired properties in a tunable manner.[29,30] Among all of the reported morphologies, LHP nanowires (NWs) have attracted a great amount of attention due to their large aspect ratios and strong quantum confinements along their short dimensions.[31−34] Typical syntheses of colloidal dispersible LHP NWs largely rely on hot-injection methods through regulating the applied organic ligands to achieve one-dimensional morphology.[35,36] However, complex interplay between organic ligands and inorganic precursors at elevated temperatures often results in a nonideal morphological uniformity.[37,38] Moreover, the mandatory mass transfer process and diffusion controlled NC nucleation and growth processes further complicate its adaptability and scaling-up for large-scale material production.[39] Recently, postsynthetic transformation reactions of LHP NCs have been proven as a facile and efficient means to access nanomaterials, in particular, with thermodynamically unfavored morphologies, crystal phases, and heterocompositions/structures.[40−51] In this context, zero-dimensional (0D) Cs_4PbX_6 (X = Cl, Br, I) perovskites are a group of perovskite analogues that are composed of isolated lead-halide ($[PbX_6]^{4-}$) octahedra in the crystal lattice.[52−54] Because of the lead-depleted stoichiometry, the 0D Cs_4PbX_6 LHP NCs can serve as ideal starting materials to react with PbX_2 and transform into three-dimensional (3D) $CsPbX_3$ LHP NCs.[40−43] However, the products from such postsynthetic transformation reactions have been largely limited to LHP NCs with more isotropic morphologies, i.e., nanocubes.[40,44]

Herein, we report the synthesis of ultrathin $CsPbBr_3$ NWs via a postsynthetic transformation reaction of 0D Cs_4PbBr_6

Received: January 31, 2021
Revised: February 22, 2021
Published: March 1, 2021

https://dx.doi.org/10.1021/acs.cgd.1c00118
Cryst. Growth Des. 2021, 21, 1924−1930

LHP NCs (Scheme 1). The ultrathin NWs showed an average diameter of 2.5 ± 0.6 nm with the wire length of tens of micrometers. Strong quantum confinement along the short dimension of the NWs leads to a blue emission peak centered at 432 nm with a PL QY of 15.2%. Interestingly, we discovered that the $PbBr_2$ precursor used for the transformation reaction can interact with the organic ligands forming lamellar-type $PbBr_2$-ligand intermediates, which can further dictate the morphological purity of the final $CsPbBr_3$ products. We also expand this postsynthetic transformation method to the case of I-containing perovskite NCs.

Scheme 1. Illustration of the Transformation Reaction from 0D Cs_4PbBr_6 Perovskite NCs to $CsPbBr_3$ LHP NWs or Nanocubes

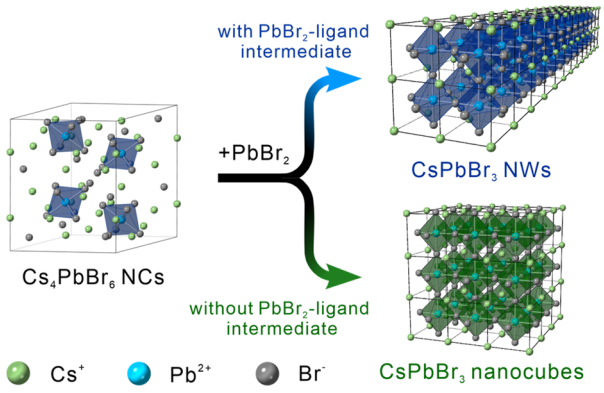

It has been reported that the lead-depleted 0D Cs_4PbBr_6 perovskite NCs can be transformed into 3D $CsPbBr_3$ perovskite nanocubes upon the addition of the $PbBr_2$ precursor.[40] Also inspired by the short organic ligand induced $CsPbBr_3$ NW formation in hot injection synthesis,[35] we propose that short alkyl chain ligands can also be used to regulate perovskite NC product morphologies for postsynthetic transformation reactions. Following this idea, we conducted perovskite NC transformation reactions in the presence of short alkyl chain organic ligands. In detail, a hexane solution of spherical Cs_4PbBr_6 NCs with an average diameter of 12.1 ± 1.0 nm was used as a starting material for the transformation reaction (Figure 1a,b and Figure S1).[40] Upon adding solid $PbBr_2$ precursors and two short alkyl chain ligands (i.e., hexanoic acid, HA and octylamine, OctAm) in addition to the commonly used oleic acid (OA) (see details in the Supporting Information), the reaction was then monitored by UV−vis absorption and PL spectroscopic measurements. A gradual emergence (disappearance) of a new absorption peak at 426 nm (the original absorption feature at 315 nm of the Cs_4PbBr_6 NCs) was observed (Figure 1a). Along with the absorption profile change, a strong blue PL peak centered at 432 nm appeared which can be assigned to excitonic emission of the formed $CsPbBr_3$ LHP NWs with strong quantum confinement (Figure 1a).[36,55] The well-defined absorption feature and the narrow emission peak (full-width at half-maximum, fwhm of ∼79 meV) proved the morphological uniformity of the product.[35] TEM images unambiguously showed the formation of ultrathin NWs with an average width of 2.5 ± 0.6 nm and more than 10 μm in length (Figure 1b−d). Low-magnification TEM images revealed that the NWs tend to form bundles due to the strong inter-NW van der Waals interactions (Figure 1e).[56] Interestingly, TEM images for the samples taken during the transformation reaction showed coexistence of both the pristine spherical Cs_4PbBr_6 NCs and the newly formed $CsPbBr_3$ LHP NWs, suggesting a dissolve-then-reform mechanism of the transformation reaction.[43] Furthermore, the width of the NWs (2.5 nm, ∼4−5 unit-cell layers) is much smaller than the estimated $CsPbBr_3$ Bohr diameter of ∼7 nm,[57] suggesting a strong exciton quantum confinement effect, which is consistent with the observed absorption and PL profiles in a much bluer region

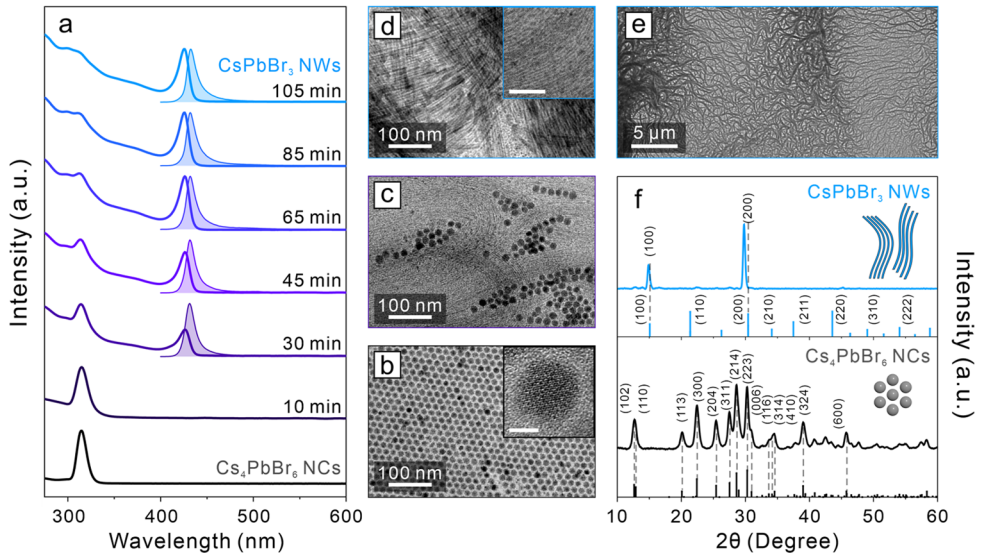

Figure 1. (a) Evolutions of the absorption (lines) and PL spectra (lines with shades) of the transformation reaction. (b−d) TEM images of (b) starting 0D Cs_4PbBr_6 perovskite NCs, (c) a mixture of Cs_4PbBr_6 NCs and newly formed $CsPbBr_3$ NWs for the sample taken at 65 min, and (d) the final $CsPbBr_3$ LHP NWs. Inset in (b): HR-TEM image of the Cs_4PbBr_6 NCs (scale bar: 5 nm). Inset in (d): zoomed-in TEM image of the $CsPbBr_3$ NW (scale bar: 50 nm). (e) Low-magnification TEM image showing a large area of the NW bundles. (f) XRD patterns of the starting 0D Cs_4PbBr_6 perovskite NCs (bottom, black) and the resulting $CsPbBr_3$ LHP NWs (top, blue). Bars represent the corresponding standard diffraction patterns.

https://dx.doi.org/10.1021/acs.cgd.1c00118
Cryst. Growth Des. 2021, 21, 1924−1930

than those from $CsPbBr_3$ nanocubes.[57] XRD patterns of the starting sample and the resulting product clearly displayed the crystal structure change from the 0D Cs_4PbBr_6 to the 3D $CsPbBr_3$ perovskite structure (Scheme 1 and Figure 1f). In addition, the $CsPbBr_3$ NWs showed a strong orientation alignment on the substrate (showing exclusively a set of {*h*00} Bragg diffraction peaks in the XRD pattern, Figure 1f), in line with the highly anisotropic 1D shape and the preferred [100] growth direction of the $CsPbBr_3$ NWs.[35,58] The slight shifts to smaller angles of the diffraction signals can be explained by a large fraction of surface exposed atoms of the NWs and lattice expansion induced by the surface capping ligand as reported previously.[59]

Optical properties of the final purified $CsPbBr_3$ LHP NWs are summarized in Figure 2. The pronounced and well-defined

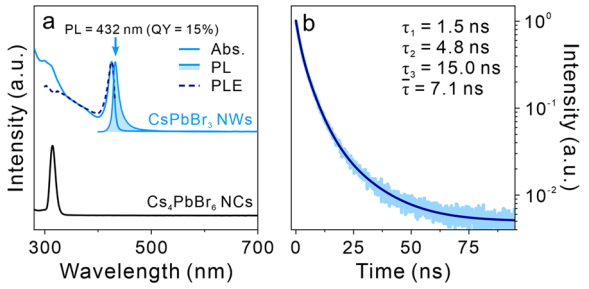

Figure 2. (a) Absorption (solid lines), PL (solid line with shade), and PLE (dashed line) spectra of the starting Cs_4PbBr_6 NCs and the resulting $CsPbBr_3$ NWs. (b) TR-PL lifetime decay curve (light blue) and the triexponential fitting line (dark blue) of the $CsPbBr_3$ LHP NWs.

absorption feature indicated a large exciton binding energy of the $CsPbBr_3$ NWs, in good accordance with the strong confinement due to the ultrathin NW morphology.[60] The PL excitation (PLE) profile closely matched the absorption spectrum of the $CsPbBr_3$ NWs, confirming that the emission at 432 nm originated from the band-edge electronic transition of the $CsPbBr_3$ NWs (Figure 2a). A PL QY of 15.2% determined by an integrating sphere technique was obtained for the sample, which was comparable to that of the NWs synthesized using a hot-injection method.[35,59] Time resolved PL (TR-PL) measurements revealed a relatively long PL decay lifetime (average lifetime of 7.1 ns) compared with directly synthesized $CsPbBr_3$ NWs with a similar band gap energy, which was likely due to the improved ligand coverage and/or decreased defect density due to the mild reaction condition (Figure 2b, Table S1).[35,61]

It is known that ligands play an imperative role in determining the final perovskite NC morphology during the synthesis.[29,38] Given the low solubility of $PbBr_2$ precursor as an inorganic salt in the nonpolar solvent (e.g., toluene), we speculate that the NW formation mechanism is likely controlled by the structure of the $PbBr_2$-ligand intermediates that transfer the $PbBr_2$ precursor into the reaction solution. To test this speculation, we synthesized various $PbBr_2$-ligand intermediates by reacting $PbBr_2$ solid precursor with different ligand combinations in toluene (see Supporting Information for details). The XRD patterns of all the synthesized $PbBr_2$-ligand intermediates showed a lamellar structure, evidenced by showing exclusively a set of {00*l*} diffraction peaks (Figure 3a, Table S2).[62] Interestingly, a good correlation between the interlayer *d*-spacing of the intermediates and the product morphology of the transformation reaction can be observed (Figure 3b). In general, for the ligand combinations that result in $PbBr_2$-ligand intermediates with large *d*-spacings (i.e., 41.7 Å for OA/OAm, 37.0 Å for HA/OAm, 29.0 and 21.5 Å for OA/OctAM), the corresponding transformation reactions led to the formation of both NWs and nanocubes (Figure 3, Figure S2).

For the ligand combinations resulting in $PbBr_2$-ligand intermediates with short *d*-spacings (e.g., 22.5 Å for HA/OctAm, 24.3 Å for HA/OA/OctAm), the transformation reactions led to the formation of solely ultrathin NWs (Figure 1, Figure 3, and Figure S2). On the basis of these results, we hypothesize that the $PbBr_2$-ligand intermediates with lamellar structures may serve as an anisotropic template to direct the growth of $CsPbBr_3$ perovskite NWs (Figure 3c). To test our hypothesis, the chain-type amine ligands were replaced by a bulky branched trioctylamine (TOAm) ligand to cease the formation of anisotropic templates of layered $PbBr_2$-ligand intermediates (Figure 3).[63] Indeed, solely $CsPbBr_3$ perovskite nanocubes without the presence of any NWs were formed, which was evidenced by both optical and TEM measurements (Figure 4a–c). The resulting $CsPbBr_3$ nanocubes showed a characteristic PL peak at 515 nm with a high PL QY of 65.3%. TR-PL revealed a long PL decay lifetime of 57.0 ns (Figure 4d, Table S1), indicating its good surface passivation.[64,65] The

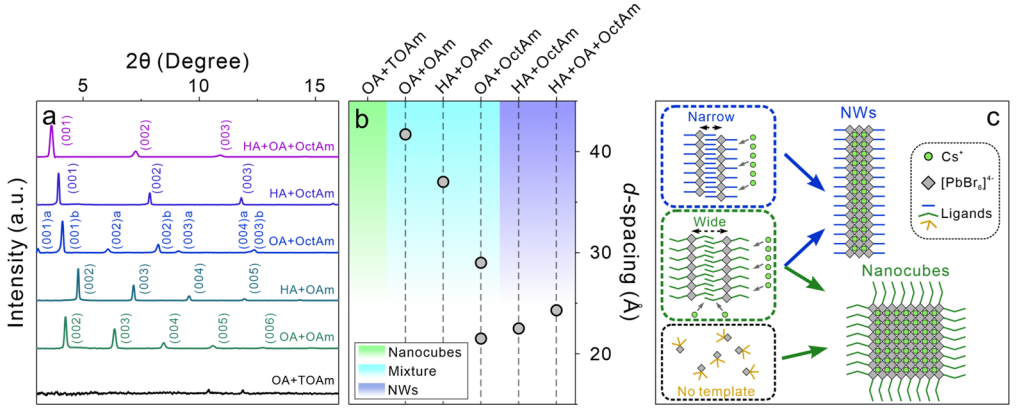

Figure 3. (a) Small-angle XRD patterns of the $PbBr_2$-ligand intermediates. Representative peaks in the XRD patterns are labeled. (b) The correlation between *d*-spacing of the $PbBr_2$-ligand intermediates and the morphology of the transformation product. (c) Schematic illustration of the template-based $CsPbBr_3$ NW and/or nanocube formation mechanism.

https://dx.doi.org/10.1021/acs.cgd.1c00118
Cryst. Growth Des. 2021, 21, 1924–1930

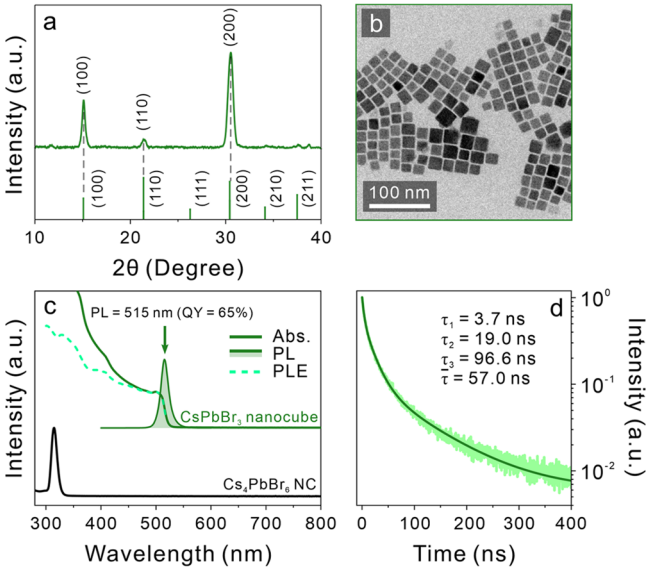

Figure 4. (a) XRD pattern and (b) TEM image of the obtained $CsPbBr_3$ nanocubes by transformation reaction. (c) The absorption (solid lines), PL (solid line with shade), and PLE (dashed line) spectra of the starting 0D Cs_4PbBr_6 perovskite NCs and the resulting $CsPbBr_3$ LHP nanocubes. (d) TR-PL decay curve (light green) and the triexponential fitting line (dark green) of the $CsPbBr_3$ nanocubes.

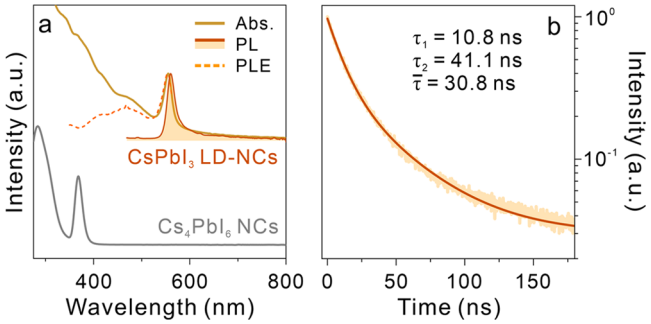

Figure 5. (a) The absorption spectra (gray and brown lines), PL spectrum (red line), and PLE spectra (orange dashed line) of the Cs_4PbI_6 NCs and the $CsPbI_3$ LD-NCs synthesized by transformation reaction. (b) TR-PL spectra of the transformed $CsPbI_3$ LD-NCs. The experimental curve is shown in the light orange line, and the biexponential fitting curve is shown in the red line.

much shorter lifetime of the NW sample (i.e., 7.1 ns) than that of the nanocubes (i.e., 57.0 ns) is due to the morphology-induced strong exciton binding energy with an enhanced quantum confinement along the short dimension of the NWs. Importantly, this result proved the necessity of $PbBr_2$-ligand intermediate-based anisotropic templates to the formation of perovskite NWs in the transformation reactions, supporting the template-mediated reaction mechanism as we proposed (Figure 3c).

To expand the scope of the reaction, we further explored the transformation reactions using 0D Cs_4PbI_6 perovskite NCs as the starting material (Figure S3).[40] Similar to the Br-containing case, the $CsPbI_3$ products can be obtained through transforming Cs_4PbI_6 NCs by adding PbI_2 precursor with both short-chain (i.e., HA and OctAm) and long-chain organic ligands (i.e., OAm, see experimental details in the Supporting Information). The disappearance of the pristine absorption peak at 369 nm originated from Cs_4PbI_6 NCs indicated completeness of the transformation reaction (Figure 5a). The newly formed $CsPbI_3$ products showed a defined absorption feature at 554 nm and a narrow PL peak centered at 560 nm (fwhm of ~83 meV), both of which were ~100 nm bluer than those of the $CsPbI_3$ nanocubes, supporting its low-dimensional (LD) morphology (either NWs or nanoplatelets) with a strong exciton confinement along the short dimension.[66,67] The obtained $CsPbI_3$ LD-NCs showed a PL QY of ~3% and a PL lifetime of 30.8 ns (Figure 5b, Table S1), ~1.4 times longer than that of the $CsPbI_3$ NWs (~22 ns) and $CsPbI_3$ nanoplatelets (10–23 ns) synthesized directly.[68−71] Because of the sample instability and quick degradation to the δ-phase of $CsPbI_3$ within minutes (Figure S4), we were unable to obtain reasonable TEM images to unambiguously determine the particle morphology. Studies on improving the sample stability are currently undergoing.

In conclusion, we report a facile synthetic method to achieve ultrathin $CsPbBr_3$ LHP NWs through a colloidal transformation reaction from 0D Cs_4PbBr_6 perovskite NCs. These NWs possess a sharp PL peak at 432 nm and a reasonable PL QY of 15.2%. Importantly, we show that the compact $PbBr_2$-ligand intermediates can serve as an effective anisotropic template and promote the formation of NWs with morphological purity. We further demonstrate that this postsynthetic transformation reaction scheme can be extended to the I-containing case. Our study not only provides a novel approach toward morphological and crystal structural controls of LHP NCs but also offers insights for future fabrications of other types of perovskite materials through nonclassical crystal nucleation and growth pathways.

■ ASSOCIATED CONTENT

Supporting Information

The Supporting Information is available free of charge at https://pubs.acs.org/doi/10.1021/acs.cgd.1c00118.

Experimental details, additional TEM images, additional absorption and PL spectra (PDF)

■ AUTHOR INFORMATION

Corresponding Author

Ou Chen − *Department of Chemistry, Brown University, Providence, Rhode Island 02912, United States;* orcid.org/0000-0003-0551-090X; Email: ouchen@brown.edu

Authors

Hanjun Yang − *Department of Chemistry, Brown University, Providence, Rhode Island 02912, United States*

Tong Cai − *Department of Chemistry, Brown University, Providence, Rhode Island 02912, United States;* orcid.org/0000-0002-4468-6767

Lacie Dube − *Department of Chemistry, Brown University, Providence, Rhode Island 02912, United States*

Katie Hills-Kimball − *Department of Chemistry, Brown University, Providence, Rhode Island 02912, United States*

Complete contact information is available at: https://pubs.acs.org/10.1021/acs.cgd.1c00118

Funding

O.C. acknowledges support from the Brown University startup fund, the 3M Nontenured Faculty Award fund, and the Camille & Henry Dreyfus Foundation through the Camille

Dreyfus Teacher-Scholar Awards program. O.C. also acknowledges the National Science Foundation (DMR-1943930, CBET-1936223). K.H.-K. is supported by the U.S. Department of Education GAANN research fellowship (P200A150037). L.D. acknowledges support from the Brown IMSD fellowship program through NIGMS (R25GM083270).

Notes

The authors declare no competing financial interest.

■ ACKNOWLEDGMENTS

O.C. acknowledges the support for TEM and XRD measurements performed at the Electron Microscopy Facility and NanoTools Facility at the Institute for Molecular and Nanoscale Innovation (IMNI) at Brown University

■ REFERENCES

(1) Kojima, A.; Teshima, K.; Shirai, Y.; Miyasaka, T. Organometal Halide Perovskites as Visible-Light Sensitizers for Photovoltaic Cells. *J. Am. Chem. Soc.* **2009**, *131* (17), 6050−6051.

(2) Lee, M. M.; Teuscher, J.; Miyasaka, T.; Murakami, T. N.; Snaith, H. J. Efficient Hybrid Solar Cells Based on Meso-Superstructured Organometal Halide Perovskites. *Science* **2012**, *338* (6107), 643−647.

(3) Burschka, J.; Pellet, N.; Moon, S.-J.; Humphry-Baker, R.; Gao, P.; Nazeeruddin, M. K.; Grätzel, M. Sequential deposition as a route to high-performance perovskite-sensitized solar cells. *Nature* **2013**, *499* (7458), 316−319.

(4) Que, M.; Dai, Z.; Yang, H.; Zhu, H.; Zong, Y.; Que, W.; Padture, N. P.; Zhou, Y.; Chen, O. Quantum-Dot-Induced Cesium-Rich Surface Imparts Enhanced Stability to Formamidinium Lead Iodide Perovskite Solar Cells. *ACS Energy Lett.* **2019**, *4* (8), 1970−1975.

(5) Yang, H.; Zhang, Y.; Hills-Kimball, K.; Zhou, Y.; Chen, O. Building bridges between halide perovskite nanocrystals and thin-film solar cells. *Sustainable Energy Fuels* **2018**, *2* (11), 2381−2397.

(6) Kim, Y.-H.; Cho, H.; Heo, J. H.; Kim, T.-S.; Myoung, N.; Lee, C.-L.; Im, S. H.; Lee, T.-W. Multicolored Organic/Inorganic Hybrid Perovskite Light-Emitting Diodes. *Adv. Mater.* **2015**, *27* (7), 1248−1254.

(7) Stranks, S. D.; Snaith, H. J. Metal-halide perovskites for photovoltaic and light-emitting devices. *Nat. Nanotechnol.* **2015**, *10* (5), 391−402.

(8) Luo, J.; Wang, X.; Li, S.; Liu, J.; Guo, Y.; Niu, G.; Yao, L.; Fu, Y.; Gao, L.; Dong, Q.; Zhao, C.; Leng, M.; Ma, F.; Liang, W.; Wang, L.; Jin, S.; Han, J.; Zhang, L.; Etheridge, J.; Wang, J.; Yan, Y.; Sargent, E. H.; Tang, J. Efficient and stable emission of warm-white light from lead-free halide double perovskites. *Nature* **2018**, *563* (7732), 541−545.

(9) Dou, L.; Yang, Y.; You, J.; Hong, Z.; Chang, W.-H.; Li, G.; Yang, Y. Solution-processed hybrid perovskite photodetectors with high detectivity. *Nat. Commun.* **2014**, *5* (1), 5404.

(10) Saidaminov, M. I.; Adinolfi, V.; Comin, R.; Abdelhady, A. L.; Peng, W.; Dursun, I.; Yuan, M.; Hoogland, S.; Sargent, E. H.; Bakr, O. M. Planar-integrated single-crystalline perovskite photodetectors. *Nat. Commun.* **2015**, *6* (1), 8724.

(11) Cai, T.; Shi, W.; Hwang, S.; Kobbekaduwa, K.; Nagaoka, Y.; Yang, H.; Hills-Kimball, K.; Zhu, H.; Wang, J.; Wang, Z.; Liu, Y.; Su, D.; Gao, J.; Chen, O. Lead-Free $Cs_4CuSb_2Cl_{12}$ Layered Double Perovskite Nanocrystals. *J. Am. Chem. Soc.* **2020**, *142* (27), 11927−11936.

(12) Yakunin, S.; Sytnyk, M.; Kriegner, D.; Shrestha, S.; Richter, M.; Matt, G. J.; Azimi, H.; Brabec, C. J.; Stangl, J.; Kovalenko, M. V.; Heiss, W. Detection of X-ray photons by solution-processed lead halide perovskites. *Nat. Photonics* **2015**, *9* (7), 444−449.

(13) Kim, Y. C.; Kim, K. H.; Son, D.-Y.; Jeong, D.-N.; Seo, J.-Y.; Choi, Y. S.; Han, I. T.; Lee, S. Y.; Park, N.-G. Printable organometallic perovskite enables large-area, low-dose X-ray imaging. *Nature* **2017**, *550* (7674), 87−91.

(14) Zhang, H.; Wang, X.; Liao, Q.; Xu, Z.; Li, H.; Zheng, L.; Fu, H. Embedding Perovskite Nanocrystals into a Polymer Matrix for Tunable Luminescence Probes in Cell Imaging. *Adv. Funct. Mater.* **2017**, *27* (7), 1604382.

(15) Meinardi, F.; Akkerman, Q. A.; Bruni, F.; Park, S.; Mauri, M.; Dang, Z.; Manna, L.; Brovelli, S. Doped Halide Perovskite Nanocrystals for Reabsorption-Free Luminescent Solar Concentrators. *ACS Energy Lett.* **2017**, *2* (10), 2368−2377.

(16) Luo, X.; Ding, T.; Liu, X.; Liu, Y.; Wu, K. Quantum-Cutting Luminescent Solar Concentrators Using Ytterbium-Doped Perovskite Nanocrystals. *Nano Lett.* **2019**, *19* (1), 338−341.

(17) Cai, T.; Wang, J.; Li, W.; Hills-Kimball, K.; Yang, H.; Nagaoka, Y.; Yuan, Y.; Zia, R.; Chen, O. Mn^{2+}/Yb^{3+} Codoped $CsPbCl_3$ Perovskite Nanocrystals with Triple-Wavelength Emission for Luminescent Solar Concentrators. *Adv. Sci.* **2020**, *7* (18), 2001317.

(18) Yuan, Y.; Zhu, H.; Hills-Kimball, K.; Cai, T.; Shi, W.; Wei, Z.; Yang, H.; Candler, Y.; Wang, P.; He, J.; Chen, O. Stereoselective C−C Oxidative Coupling Reactions Photocatalyzed by Zwitterionic Ligand Capped $CsPbBr_3$ Perovskite Quantum Dots. *Angew. Chem., Int. Ed.* **2020**, *59* (50), 22563−22569.

(19) Manser, J. S.; Christians, J. A.; Kamat, P. V. Intriguing Optoelectronic Properties of Metal Halide Perovskites. *Chem. Rev.* **2016**, *116* (21), 12956−13008.

(20) Akkerman, Q. A.; D'Innocenzo, V.; Accornero, S.; Scarpellini, A.; Petrozza, A.; Prato, M.; Manna, L. Tuning the Optical Properties of Cesium Lead Halide Perovskite Nanocrystals by Anion Exchange Reactions. *J. Am. Chem. Soc.* **2015**, *137* (32), 10276−10281.

(21) Nedelcu, G.; Protesescu, L.; Yakunin, S.; Bodnarchuk, M. I.; Grotevent, M. J.; Kovalenko, M. V. Fast Anion-Exchange in Highly Luminescent Nanocrystals of Cesium Lead Halide Perovskites ($CsPbX_3$, X = Cl, Br, I). *Nano Lett.* **2015**, *15* (8), 5635−5640.

(22) Liu, W.; Lin, Q.; Li, H.; Wu, K.; Robel, I.; Pietryga, J. M.; Klimov, V. I. Mn^{2+}-Doped Lead Halide Perovskite Nanocrystals with Dual-Color Emission Controlled by Halide Content. *J. Am. Chem. Soc.* **2016**, *138* (45), 14954−14961.

(23) Cai, T.; Yang, H.; Hills-Kimball, K.; Song, J.-P.; Zhu, H.; Hofman, E.; Zheng, W.; Rubenstein, B. M.; Chen, O. Synthesis of All-Inorganic Cd-Doped $CsPbCl_3$ Perovskite Nanocrystals with Dual-Wavelength Emission. *J. Phys. Chem. Lett.* **2018**, *9* (24), 7079−7084.

(24) Koscher, B. A.; Swabeck, J. K.; Bronstein, N. D.; Alivisatos, A. P. Essentially Trap-Free $CsPbBr_3$ Colloidal Nanocrystals by Postsynthetic Thiocyanate Surface Treatment. *J. Am. Chem. Soc.* **2017**, *139* (19), 6566−6569.

(25) Hu, F.; Zhang, H.; Sun, C.; Yin, C.; Lv, B.; Zhang, C.; Yu, W. W.; Wang, X.; Zhang, Y.; Xiao, M. Superior Optical Properties of Perovskite Nanocrystals as Single Photon Emitters. *ACS Nano* **2015**, *9* (12), 12410−12416.

(26) Rainò, G.; Becker, M. A.; Bodnarchuk, M. I.; Mahrt, R. F.; Kovalenko, M. V.; Stöferle, T. Superfluorescence from lead halide perovskite quantum dot superlattices. *Nature* **2018**, *563* (7733), 671−675.

(27) Isarov, M.; Tan, L. Z.; Bodnarchuk, M. I.; Kovalenko, M. V.; Rappe, A. M.; Lifshitz, E. Rashba Effect in a Single Colloidal $CsPbBr_3$ Perovskite Nanocrystal Detected by Magneto-Optical Measurements. *Nano Lett.* **2017**, *17* (8), 5020−5026.

(28) Ramade, J.; Andriambariarijaona, L. M.; Steinmetz, V.; Goubet, N.; Legrand, L.; Barisien, T.; Bernardot, F.; Testelin, C.; Lhuillier, E.; Bramati, A.; Chamarro, M. Fine structure of excitons and electron−hole exchange energy in polymorphic $CsPbBr_3$ single nanocrystals. *Nanoscale* **2018**, *10* (14), 6393−6401.

(29) Pan, A. Z.; He, B.; Fan, X. Y.; Liu, Z. K.; Urban, J. J.; Alivisatos, A. P.; He, L.; Liu, Y. Insight into the Ligand-Mediated Synthesis of Colloidal CsPbBr3 Perovskite Nanocrystals: The Role of Organic Acid, Base, and Cesium Precursors. *ACS Nano* **2016**, *10* (8), 7943−7954.

(30) Bekenstein, Y.; Koscher, B. A.; Eaton, S. W.; Yang, P. D.; Alivisatos, A. P. Highly Luminescent Colloidal Nanoplates of Perovskite Cesium Lead Halide and Their Oriented Assemblies. *J. Am. Chem. Soc.* **2015**, *137* (51), 16008−16011.

https://dx.doi.org/10.1021/acs.cgd.1c00118
Cryst. Growth Des. 2021, 21, 1924−1930

(31) Zhu, H. M.; Fu, Y. P.; Meng, F.; Wu, X. X.; Gong, Z. Z.; Ding, Q.; Gustafsson, M. V.; Trinh, M. T.; Jin, S.; Zhu, X. Y. Lead halide perovskite nanowire lasers with low lasing thresholds and high quality factors. *Nat. Mater.* **2015**, *14* (6), 636−642.
(32) Eaton, S. W.; Lai, M. L.; Gibson, N. A.; Wong, A. B.; Dou, L. T.; Ma, J.; Wang, L. W.; Leone, S. R.; Yang, P. D. Lasing in robust cesium lead halide perovskite nanowires. *Proc. Natl. Acad. Sci. U. S. A.* **2016**, *113* (8), 1993−1998.
(33) Gao, L.; Zeng, K.; Guo, J. S.; Ge, C.; Du, J.; Zhao, Y.; Chen, C.; Deng, H.; He, Y. S.; Song, H. S.; Niu, G. D.; Tang, J. Passivated Single-Crystalline $CH_3NH_3PbI_3$ Nanowire Photodetector with High Detectivity and Polarization Sensitivity. *Nano Lett.* **2016**, *16* (12), 7446−7454.
(34) Zhang, Y.; Yang, H.; Chen, M.; Padture, N. P.; Chen, O.; Zhou, Y. Fusing Nanowires into Thin Films: Fabrication of Graded-Heterojunction Perovskite Solar Cells with Enhanced Performance. *Adv. Energy Mater.* **2019**, *9* (22), 1900243.
(35) Imran, M.; Di Stasio, F.; Dang, Z. Y.; Canale, C.; Khan, A. H.; Shamsi, J.; Brescia, R.; Prato, M.; Manna, L. Colloidal Synthesis of Strongly Fluorescent $CsPbBr_3$ Nanowires with Width Tunable down to the Quantum Confinement Regime. *Chem. Mater.* **2016**, *28* (18), 6450−6454.
(36) Zhang, D. D.; Yu, Y.; Bekenstein, Y.; Wong, A. B.; Alivisatos, A. P.; Yang, P. D. Ultrathin Colloidal Cesium Lead Halide Perovskite Nanowires. *J. Am. Chem. Soc.* **2016**, *138* (40), 13155−13158.
(37) Parobek, D.; Dong, Y.; Qiao, T.; Son, D. H. Direct Hot-Injection Synthesis of Mn-Doped $CsPbBr_3$ Nanocrystals. *Chem. Mater.* **2018**, *30* (9), 2939−2944.
(38) Liang, Z. Q.; Zhao, S. L.; Xu, Z.; Qiao, B.; Song, P. J.; Gao, D.; Xu, X. R. Shape-Controlled Synthesis of All-Inorganic $CsPbBr_3$ Perovskite Nanocrystals with Bright Blue Emission. *ACS Appl. Mater. Interfaces* **2016**, *8* (42), 28824−28830.
(39) De Nolf, K.; Capek, R. K.; Abe, S.; Sluydts, M.; Jang, Y.; Martins, J. C.; Cottenier, S.; Lifshitz, E.; Hens, Z. Controlling the Size of Hot Injection Made Nanocrystals by Manipulating the Diffusion Coefficient of the Solute. *J. Am. Chem. Soc.* **2015**, *137* (7), 2495−2505.
(40) Akkerman, Q. A.; Park, S.; Radicchi, E.; Nunzi, F.; Mosconi, E.; De Angelis, F.; Brescia, R.; Rastogi, P.; Prato, M.; Manna, L. Nearly Monodisperse Insulator Cs_4PbX_6 (X = Cl, Br, I) Nanocrystals, Their Mixed Halide Compositions, and Their Transformation into $CsPbX_3$ Nanocrystals. *Nano Lett.* **2017**, *17* (3), 1924−1930.
(41) Palazon, F.; Almeida, G.; Akkerman, Q. A.; De Trizio, L.; Dang, Z.; Prato, M.; Manna, L. Changing the Dimensionality of Cesium Lead Bromide Nanocrystals by Reversible Postsynthesis Transformations with Amines. *Chem. Mater.* **2017**, *29* (10), 4167−4171.
(42) Hu, H.; Wu, L.; Tan, Y.; Zhong, Q.; Chen, M.; Qiu, Y.; Yang, D.; Sun, B.; Zhang, Q.; Yin, Y. Interfacial Synthesis of Highly Stable CsPbX3/Oxide Janus Nanoparticles. *J. Am. Chem. Soc.* **2018**, *140* (1), 406−412.
(43) Li, Y.; Huang, H.; Xiong, Y.; Kershaw, S. V.; Rogach, A. L. Reversible transformation between $CsPbBr_3$ and Cs_4PbBr_6 nanocrystals. *CrystEngComm* **2018**, *20* (34), 4900−4904.
(44) Wu, L.; Hu, H.; Xu, Y.; Jiang, S.; Chen, M.; Zhong, Q.; Yang, D.; Liu, Q.; Zhao, Y.; Sun, B.; Zhang, Q.; Yin, Y. From Nonluminescent Cs_4PbX_6 (X = Cl, Br, I) Nanocrystals to Highly Luminescent $CsPbX_3$ Nanocrystals: Water-Triggered Transformation through a CsX-Stripping Mechanism. *Nano Lett.* **2017**, *17* (9), 5799−5804.
(45) Palazon, F.; Urso, C.; De Trizio, L.; Akkerman, Q.; Marras, S.; Locardi, F.; Nelli, I.; Ferretti, M.; Prato, M.; Manna, L. Postsynthesis Transformation of Insulating Cs_4PbBr_6 Nanocrystals into Bright Perovskite $CsPbBr_3$ through Physical and Chemical Extraction of CsBr. *ACS Energy Lett.* **2017**, *2* (10), 2445−2448.
(46) Nagaoka, Y.; Hills-Kimball, K.; Tan, R.; Li, R.; Wang, Z.; Chen, O. Nanocube Superlattices of Cesium Lead Bromide Perovskites and Pressure-Induced Phase Transformations at Atomic and Mesoscale Levels. *Adv. Mater.* **2017**, *29* (18), 1606666.
(47) Hills-Kimball, K.; Nagaoka, Y.; Cao, C.; Chaykovsky, E.; Chen, O. Synthesis of formamidinium lead halide perovskite nanocrystals through solid−liquid−solid cation exchange. *J. Mater. Chem. C* **2017**, *5* (23), 5680−5684.
(48) Yu, X.; Wu, L.; Hu, H.; Chen, M.; Tan, Y.; Yang, D.; Pan, Q.; Zhong, Q.; Supasai, T.; Zhang, Q. Cs_4PbX_6 (X = Cl, Br, I) Nanocrystals: Preparation, Water-Triggered Transformation Behavior, and Anti-Counterfeiting Application. *Langmuir* **2018**, *34* (35), 10363−10370.
(49) Zhu, H.; Cai, T.; Que, M.; Song, J.-P.; Rubenstein, B. M.; Wang, Z.; Chen, O. Pressure-Induced Phase Transformation and Band-Gap Engineering of Formamidinium Lead Iodide Perovskite Nanocrystals. *J. Phys. Chem. Lett.* **2018**, *9* (15), 4199−4205.
(50) Yang, H.; Cai, T.; Liu, E.; Hills-Kimball, K.; Gao, J.; Chen, O. Synthesis and transformation of zero-dimensional Cs_3BiX_6 (X = Cl, Br) perovskite-analogue nanocrystals. *Nano Res.* **2020**, *13* (1), 282−291.
(51) Hills-Kimball, K.; Pérez, M. J.; Nagaoka, Y.; Cai, T.; Yang, H.; Davis, A. H.; Zheng, W.; Chen, O. Ligand Engineering for Mn^{2+} Doping Control in $CsPbCl_3$ Perovskite Nanocrystals via a Quasi-Solid−Solid Cation Exchange Reaction. *Chem. Mater.* **2020**, *32* (6), 2489−2500.
(52) Xiao, Z.; Meng, W.; Wang, J.; Mitzi, D. B.; Yan, Y. Searching for promising new perovskite-based photovoltaic absorbers: the importance of electronic dimensionality. *Mater. Horiz.* **2017**, *4* (2), 206−216.
(53) Zhu, J.; Di, Q.; Zhao, X.; Wu, X.; Fan, X.; Li, Q.; Song, W.; Quan, Z. Facile Method for the Controllable Synthesis of $Cs_xPb_yBr_z$-Based Perovskites. *Inorg. Chem.* **2018**, *57* (11), 6206−6209.
(54) Billstrand, B.; Bian, K.; Karler, C.; Ye, D.; Hwang, A.; Fan, H. Solution Based Synthesis of Cs_4PbBr_6 Perovskite Particles with High Luminescence and Stability. *MRS Advances* **2018**, *3* (45−46), 2825−2831.
(55) Amgar, D.; Stern, A.; Rotem, D.; Porath, D.; Etgar, L. Tunable Length and Optical Properties of $CsPbX_3$ (X = Cl, Br, I) Nanowires with a Few Unit Cells. *Nano Lett.* **2017**, *17* (2), 1007−1013.
(56) Teunis, M. B.; Jana, A.; Dutta, P.; Johnson, M. A.; Mandal, M.; Muhoberac, B. B.; Sardar, R. Mesoscale Growth and Assembly of Bright Luminescent Organolead Halide Perovskite Quantum Wires. *Chem. Mater.* **2016**, *28* (14), 5043−5054.
(57) Protesescu, L.; Yakunin, S.; Bodnarchuk, M. I.; Krieg, F.; Caputo, R.; Hendon, C. H.; Yang, R. X.; Walsh, A.; Kovalenko, M. V. Nanocrystals of Cesium Lead Halide Perovskites ($CsPbX_3$, X = Cl, Br, and I): Novel Optoelectronic Materials Showing Bright Emission with Wide Color Gamut. *Nano Lett.* **2015**, *15* (6), 3692−3696.
(58) Holder, C. F.; Schaak, R. E. Tutorial on Powder X-ray Diffraction for Characterizing Nanoscale Materials. *ACS Nano* **2019**, *13* (7), 7359−7365.
(59) Zhao, J.; Liu, M.; Fang, L.; Jiang, S.; Zhou, J.; Ding, H.; Huang, H.; Wen, W.; Luo, Z.; Zhang, Q.; Wang, X.; Gao, C. Great Disparity in Photoluminesence Quantum Yields of Colloidal $CsPbBr_3$ Nanocrystals with Varied Shape: The Effect of Crystal Lattice Strain. *J. Phys. Chem. Lett.* **2017**, *8* (13), 3115−3121.
(60) Zhang, S.; Shang, Q.; Du, W.; Shi, J.; Wu, Z.; Mi, Y.; Chen, J.; Liu, F.; Li, Y.; Liu, M.; Zhang, Q.; Liu, X. Strong Exciton−Photon Coupling in Hybrid Inorganic−Organic Perovskite Micro/Nanowires. *Adv. Opt. Mater.* **2018**, *6* (2), 1701032.
(61) Liu, Y.; Guo, M.; Dong, S.; Jiao, X.; Wang, T.; Chen, D. Room temperature colloidal synthesis of $CsPbBr_3$ nanowires with tunable length, width and composition. *J. Mater. Chem. C* **2018**, *6* (29), 7797−7802.
(62) Tan, Z.; Wu, Y.; Hong, H.; Yin, J.; Zhang, J.; Lin, L.; Wang, M.; Sun, X.; Sun, L.; Huang, Y.; Liu, K.; Liu, Z.; Peng, H. Two-Dimensional $(C_4H_9NH_3)_2PbBr_4$ Perovskite Crystals for High-Performance Photodetector. *J. Am. Chem. Soc.* **2016**, *138* (51), 16612−16615.
(63) Cho, J.; Jin, H.; Sellers, D. G.; Watson, D. F.; Son, D. H.; Banerjee, S. Influence of ligand shell ordering on dimensional

https://dx.doi.org/10.1021/acs.cgd.1c00118
Cryst. Growth Des. 2021, 21, 1924−1930

confinement of cesium lead bromide ($CsPbBr_3$) perovskite nanoplatelets. *J. Mater. Chem. C* **2017**, *5* (34), 8810−8818.
(64) Wu, Y.; Wei, C.; Li, X.; Li, Y.; Qiu, S.; Shen, W.; Cai, B.; Sun, Z.; Yang, D.; Deng, Z.; Zeng, H. In Situ Passivation of $PbBr_6^{4-}$ Octahedra toward Blue Luminescent CsPbBr3 Nanoplatelets with Near 100% Absolute Quantum Yield. *ACS Energy Lett.* **2018**, *3* (9), 2030−2037.
(65) Ravi, V. K.; Saikia, S.; Yadav, S.; Nawale, V. V.; Nag, A. $CsPbBr_3$/ZnS Core/Shell Type Nanocrystals for Enhancing Luminescence Lifetime and Water Stability. *ACS Energy Lett.* **2020**, *5* (6), 1794−1796.
(66) Swarnkar, A.; Marshall, A. R.; Sanehira, E. M.; Chernomordik, B. D.; Moore, D. T.; Christians, J. A.; Chakrabarti, T.; Luther, J. M. Quantum dot-induced phase stabilization of α-$CsPbI_3$ perovskite for high-efficiency photovoltaics. *Science* **2016**, *354* (6308), 92−95.
(67) Weidman, M. C.; Seitz, M.; Stranks, S. D.; Tisdale, W. A. Highly Tunable Colloidal Perovskite Nanoplatelets through Variable Cation, Metal, and Halide Composition. *ACS Nano* **2016**, *10* (8), 7830−7839.
(68) Chen, Z.; Dong, L.; Tang, H.; Yu, Y.; Ye, L.; Zang, J. Direct synthesis of cubic phase $CsPbI_3$ nanowires. *CrystEngComm* **2019**, *21* (9), 1389−1396.
(69) Li, Z.-J.; Hofman, E.; Davis, A. H.; Maye, M. M.; Zheng, W. General Strategy for the Growth of $CsPbX_3$ (X = Cl, Br, I) Perovskite Nanosheets from the Assembly of Nanorods. *Chem. Mater.* **2018**, *30* (11), 3854−3860.
(70) Tong, Y.; Bladt, E.; Aygüler, M. F.; Manzi, A.; Milowska, K. Z.; Hintermayr, V. A.; Docampo, P.; Bals, S.; Urban, A. S.; Polavarapu, L.; Feldmann, J. Highly Luminescent Cesium Lead Halide Perovskite Nanocrystals with Tunable Composition and Thickness by Ultrasonication. *Angew. Chem., Int. Ed.* **2016**, *55* (44), 13887−13892.
(71) Uddin, M. A.; Glover, J. D.; Park, S. M.; Pham, J. T.; Graham, K. R. Growth of Highly Stable and Luminescent $CsPbX_3$ (X = Cl, Br, and I) Nanoplates via Ligand Mediated Anion Exchange of $CsPbCl_3$ Nanocubes with AlX_3. *Chem. Mater.* **2020**, *32* (12), 5217−5225.

https://dx.doi.org/10.1021/acs.cgd.1c00118
Cryst. Growth Des. 2021, 21, 1924−1930